AIP | Applied Physics Letters

Interfacial electronic transport phenomena in single crystalline Fe-MgO-Fe thin barrier junctions

R. B. Gangineni, C. Bellouard, A. Duluard, B. Negulescu, C. Baraduc, G. Gaudin, and C. Tiusan

Citation: Applied Physics Letters **104**, 182402 (2014); doi: 10.1063/1.4875386
View online: http://dx.doi.org/10.1063/1.4875386
View Table of Contents: http://scitation.aip.org/content/aip/journal/apl/104/18?ver=pdfcov
Published by the AIP Publishing

Articles you may be interested in

Fe/MgO/Fe (100) textured tunnel junctions exhibiting spin polarization features of single crystal junctions
Appl. Phys. Lett. **100**, 072408 (2012); 10.1063/1.3687174

Correlation between symmetry-selective transport and spin-dependent resonant tunneling in fully epitaxial Cr/ultrathin-Fe/MgO/Fe(001) magnetic tunnel junctions
Appl. Phys. Lett. **99**, 182508 (2011); 10.1063/1.3647578

The interface structure and magnetic and electronic properties of a Co2FeAl0.5Si0.5/MgO/Co2FeAl0.5Si0.5 magnetic tunneling junction
J. Appl. Phys. **109**, 083509 (2011); 10.1063/1.3567300

Annealing of CoFeB/MgO based single and double barrier magnetic tunnel junctions: Tunnel magnetoresistance, bias dependence, and output voltage
J. Appl. Phys. **105**, 033916 (2009); 10.1063/1.3068186

Noise in MgO barrier magnetic tunnel junctions with CoFeB electrodes: Influence of annealing temperature
Appl. Phys. Lett. **90**, 252501 (2007); 10.1063/1.2749433

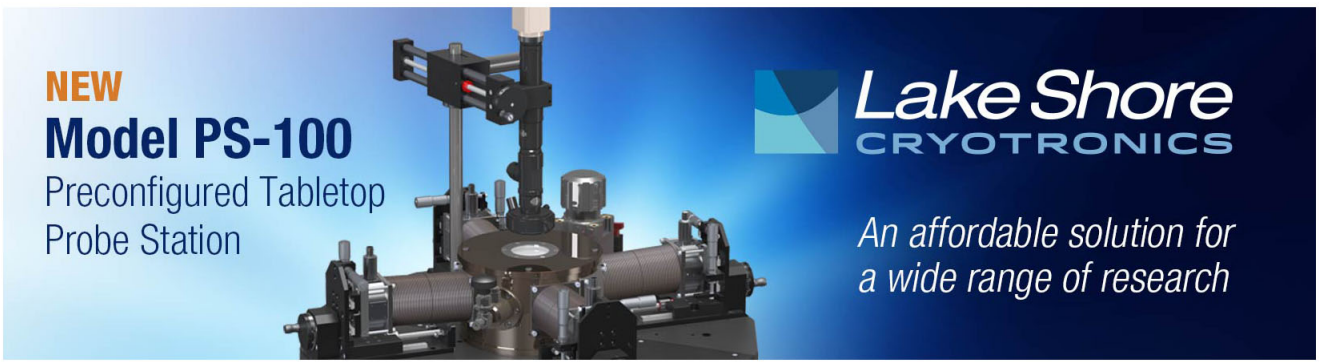

This article is copyrighted as indicated in the article. Reuse of AIP content is subject to the terms at: http://scitation.aip.org/termsconditions. Downloaded to IP: 193.226.5.148 On: Wed, 14 May 2014 07:35:56

Interfacial electronic transport phenomena in single crystalline Fe-MgO-Fe thin barrier junctions

R. B. Gangineni,[1,2,a)] C. Bellouard,[3,b)] A. Duluard,[3] B. Negulescu,[3,4] C. Baraduc,[2] G. Gaudin,[2] and C. Tiusan[3,5,c)]

[1]*Department of Physics, School of Physical, Chemical and Applied Sciences, Pondicherry University, R. V. Nagar, Kalapet, Pondicherry 605 014, India*
[2]*SPINTEC, UMR 8191 CEA/CNRS/UJF-Grenoble 1/Grenoble INP, INAC, 17 rue des Martyrs, F-38054 Grenoble Cedex, France*
[3]*Institut Jean Lamour, UMR 7198, CNRS-Université de Lorraine, BP 239, 54506 Vandoeuvre, France*
[4]*UFR de Sciences et Techniques, Matériaux, microélectronique, acoustique, nanotechnologies (GREMAN), University François Rabelais, Parc de Grandmont, 37200 Tours, France*
[5]*Department of Physics and Chemistry, Center of Superconductivity, Spintronics and Surface Science, Technical University of Cluj Napoca, Str. Memorandumului No. 28, RO-400114 Cluj-Napoca, Romania*

(Received 10 January 2014; accepted 27 April 2014; published online 5 May 2014)

Spin filtering effects in nano-pillars of Fe-MgO-Fe single crystalline magnetic tunnel junctions are explored with two different sample architectures and thin MgO barriers (thickness: 3–8 monolayers). The two architectures, with different growth and annealing conditions of the bottom electrode, allow tuning the quality of the bottom Fe/MgO interface. As a result, an interfacial resonance states (IRS) is observed or not depending on this interface quality. The IRS contribution, observed by spin polarized tunnel spectroscopy, is analyzed as a function of the MgO barrier thickness. Our experimental findings agree with theoretical predictions concerning the symmetry of the low energy (0.2 eV) interfacial resonance states: a mixture of Δ_1-like and Δ_5-like symmetries.
© *2014 AIP Publishing LLC*. [http://dx.doi.org/10.1063/1.4875386]

Theoretical works[1,2] predicted that symmetry dependent spin filtering leads to huge tunnel magnetoresistance (TMR) ratio in single crystalline magnetic tunnel junctions (MTJs). The Fe/MgO/Fe structure was found to be a model system for understanding the transport in single crystalline MTJs due to the layer by layer growth of MgO on (100) Fe surface.[3,4] Numerous experimental studies have been performed on this system in the asymptotic barrier thickness regime ($\geq$10 monolayers (MLs)), where the transport is mostly dominated by states with $k_{||} = 0$ (Δ direction in reciprocal space), and where huge TMR values are expected. Indeed, this regime is dominated by the Δ_1 symmetry channel, which is half metallic with respect to the spin channels. Nevertheless, the measured TMR ratios in such single crystalline MTJs remain limited[5–8] with respect to the theoretical prediction and to experimental results obtained with texture junctions.[9,10] Limitations of the TMR in experimental monocristalline Fe/MgO/Fe MTJs have been first associated to the presence of oxygen vacancies within the MgO barriers,[11–13] roughness of interfaces[14] or controversial Fe oxidation at Fe/MgO interfaces.[15–18] Furthermore, it has also been observed that structural defects of the barrier, attributed to misfit dislocations involved in this barrier regime, are detrimental for TMR.[19,20] Beyond these chemical and structural defects, specificity of interface electronic structure has to be taken into account in epitaxial junctions. The existence of interfacial states at the interface between Fe(100), vacuum, insulators, or semiconductor, located in the minority band above the Fermi level, has been initially theoretically predicted.[1,21,22] These states were expected to have major importance on tunneling transport.[1,24] They have been experimentally observed[23,25–27] and furthermore theoretically refined by *ab-initio* calculations within the non-equilibrium regime of a biased Fe/MgO/Fe MTJ.[28] If the symmetry character of the high energy interfacial resonance state (IRS) (1 eV) has been clearly analyzed,[26] the Bloch symmetry of the low energy IRS has been poorly investigated via spin polarized tunneling spectroscopy experiments. Theoretically, this IRS state has been first predicted to belong to Δ_1-like symmetry in the case of vacuum interface,[29] whereas a more recent study predicts a mixing of Δ_1-like and Δ_5-like symmetries at MgO interface.[30] However, symmetry channels like Δ_5, which are strongly attenuated within the single crystal barrier, are not suitably studied in the asymptotic tunnel transport regime (thick barrier junctions).

The present study is focused on the transport properties of Fe/MgO/Fe tunnel junctions at the early stage of the MgO barrier growth, with a MgO thickness between 3 and 8 monolayers. These junctions are particularly interesting for spin transfer torque applications where the manipulation of the magnetization by spin currents require tunnel currents larger than critical values.[31–33] Moreover, in contrast with thick barrier junctions, both lower spin filtering effect and better structural quality of the barrier are expected. The better structural quality of the thin barrier relates to the pseudomorphic growth of MgO strained on Fe in this thickness range. For thicker barrier, above a critical thickness,[34] dislocations appear and propagate across the whole MgO layer due the Fe/MgO lattice mismatch. Moreover, the quality of the bottom Fe/MgO interface is tuned by the sample architecture (soft or hard layer at the bottom), and specific signature of interfacial electronic structure (e.g., IRS) on tunnel

[a)]rameshg.phy@pondiuni.edu.in
[b)]christine.bellouard@ijl.nancy-universite.fr
[c)]coriolan.tiusan@phys.utcluj.ro

 © 2014 AIP Publishing LLC

This article is copyrighted as indicated in the article. Reuse of AIP content is subject to the terms at: http://scitation.aip.org/termsconditions. Downloaded to IP: 193.226.5.148 On: Wed, 14 May 2014 07:35:56

transport is explored. The present study shows that the low symmetry filtering provided by the thin MgO single crystal barrier allows to study the tunnel transport contribution of the low energy (0.2 eV) IRS with different barrier thicknesses, and analyzing its Bloch symmetry.

The MTJs are grown using molecular beam epitaxy (MBE) controlled by *in-situ* reflection high energy electron diffraction (RHEED). Two architectures of junctions have been considered, with bottom magnetic free layer (A-type): MgO//MgO-10 nm/Fe(1)-45 nm/MgO-5, 6, 7, 8 ML/Fe(2)-10 nm/Co-30 nm/Au-20 nm, and with bottom magnetic hard layer (B-type): MgO//MgO-10 nm/Cr40 nm/Co-3.5 nm/Fe(1)-2.5 nm/MgO-3, 4, 5, 6 ML/Fe(2)-7 nm/Au-20 nm. To check the MgO thickness dependence of transport characteristics for each junction type, four MgO thicknesses have been grown on the same wafer by using an *in-situ* shutter; all other growth parameters are then identical for each A or B type sample. They are denoted as A(B)-x-ML, where x states for the MgO barrier thickness expressed in ML. The structural quality and the flatness of each metallic layer have been optimized by tuning the annealing temperature and checked by RHEED. For A-samples, Fe(1) has been annealed at 450 °C (20 min). For B-samples, the Cr buffer layer has been annealed at 600 °C, whereas temperature annealing of Co and Fe(1) have been limited to 370 °C and 350 °C, respectively (10 min), to prevent the Cr-Co or Co-Fe inter-diffusion. Finally, for A- and B-samples, MgO layer has been grown at 80 °C and Fe(2) has been annealed at 220 °C for 20 min. The thicknesses of the MgO barriers are precisely controlled from RHEED oscillations as presented in Fig. 2. The static magnetic properties of the as-deposited MTJ stacks have been controlled using standard vibrating sample magnetometry. As the area resistance product (RA) of the MTJ decreases with the barrier thickness, one has to reduce the area to get junctions resistance at least in the 50 Ω range suitable for the measurement set-up. Patterning pillars with sub-micrometric lateral sizes has been performed by combined e-beam and UV-lithography and ion milling using a sputtered hard mask (Ti 5 nm/Au 130 nm/Ti 30 nm). The nano-pillars sizes are 300×100 nm^2 (A-sample) and 200×100 nm^2 (B-sample). Their transport properties have been measured with two probes and differential conductance measurements were performed with a lock-in at 1 kHz. All the magneto-transport experiments presented in this paper are performed at room temperature (RT).

Fig. 1(a) represents the schematic picture of the device contacts with bottom and top electrodes and Fig. 1(b) represents the SEM picture of a 200 nm circular nano-pillar. To ensure a monodomain magnetic configuration, measurements

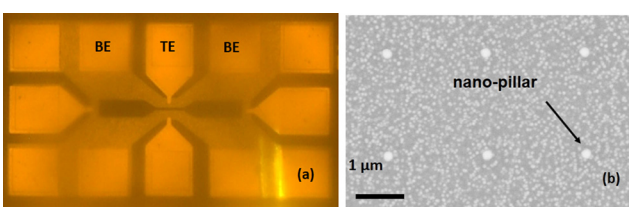

FIG. 1. (a) The schematic picture of the contacting geometry with the indication of Top (TE) and Bottom (BE) electrodes. (b) SEM picture of 200 nm diameter patterned nano-pillar.

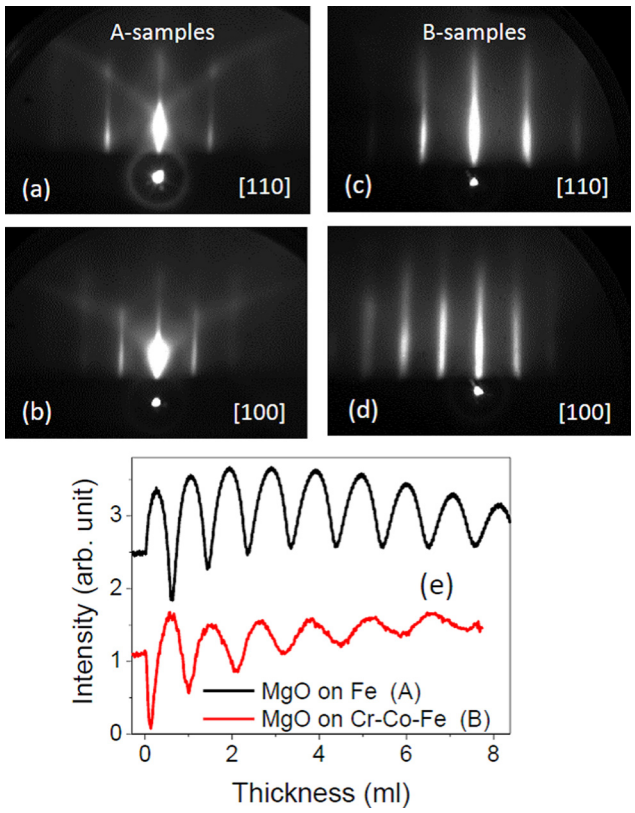

FIG. 2. RHEED diffraction patterns of bottom Fe (001) surface after annealing: (a) and (b) for A-samples; (c) and (d) for B-samples; Figure 2(e): RHEED oscillations of the MgO barrier for A and B—samples.

are carried on 300×100 nm^2 (A-sample) and or 200×100 nm^2 (B-sample) rectangular shaped nano-pillar.

Figure 2 presents RHEED diffraction patterns of the Fe(1) layer for both samples after annealing. The difference of surface quality between A and B samples is obvious. Figures 2(a) and 2(b) exhibit a bright central spot with Kikuchi lines and only first order weak diffraction rods, whereas Figures 2(c) and 2(d) show a thinner central spot with several higher order diffraction rods. These features give evidence of better flatness quality of the bottom Fe/MgO interface of A-samples with respect to B-samples, as a result of the different annealing temperatures: 450 °C compared with 350 °C. Nevertheless, RHEED oscillations during MgO growth are observed for both samples with a larger damping in the case of B-sample (Figure 2(e)), as expected from the lower quality of the initial surface. The nominal MgO thickness is estimated from the period of RHEED oscillations with an absolute uncertainty of about 0.5 ML. Moreover, we point out that no superlattice line is observed in Figure 2(a), as can be found in case of carbon contamination.[32] Thanks to the deposition of a MgO buffer layer, the bottom Fe/MgO interface in A samples is free from carbon segregation.

Figure 3 shows the Resistance per Area product (R_pA) in the parallel (G_P) magnetization configuration as a function of MgO barrier thickness for both A- and B-samples. As expected, the R_pA product increases exponentially with MgO barrier thickness. We point out that the experimental R_pA products of B-samples are globally shifted to lower values with respect to A-samples. This shift lies almost within

This article is copyrighted as indicated in the article. Reuse of AIP content is subject to the terms at: http://scitation.aip.org/termsconditions. Downloaded to IP: 193.226.5.148 On: Wed, 14 May 2014 07:35:56

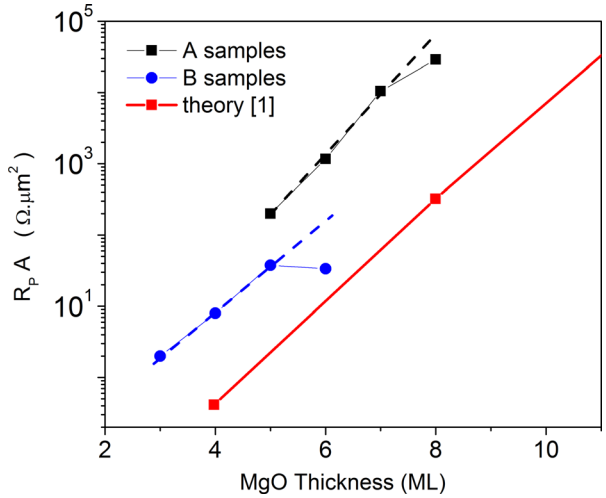

FIG. 3. Parallel resistance per junction area products (R_pA) versus MgO barrier thickness for both A and B series samples.

the MgO thickness uncertainty. However, one might correlate the higher resistance state of A-junctions with respect to B-junctions with the better quality of the barrier (roughness and thickness homogeneity). For comparison, results taken from the theoretical Density Functional Theory (DFT) calculations on Fe/MgO/Fe interfaces[1] have also been plotted in Figure 3. Interestingly, R_pA experimental values, plotted in logarithmic scale, exhibit a linear variation with a slope (dashed lines) close to the theoretical one for A-$5 \leq x \leq 7$ ML and B-$3 \leq x \leq 5$ ML samples. We point out that a deviation of $\log(R_pA)$ versus t_{MgO} from the linear dependence is observed for the thicker barrier of each sample: A-8 ML and B-6 ML exhibit a lower resistance than expected from the exponential dependence (dashed line). We will associate this deviation to a sudden decrease of the quality of the barrier, this point being addressed more in detail below.

Figures 4(a)–4(e) gather the bias voltage dependence of differential conductance $G = \frac{dI}{dV}$ measured in G_P and antiparallel (G_{AP}) magnetic configuration, TMR and derivative of G_{AP}. V_{bias} is the voltage applied to bottom electrode with respect to top: electrons flow from top to bottom electrode for positive bias. Figures 4(a) and 4(b) present the dynamical conductance of A and B samples, respectively, for the same MgO thickness (5 ML). A symmetric behavior is observed for both G_P and G_{AP} versus V_{bias} for B-sample with a stronger increase of conductance with voltage in the AP state. On the contrary, an asymmetric behavior is observed in the case of A-sample, particularly in $G_{ap}(V)$ with a peculiar feature where G_{ap} crosses G_P for voltages above 0.15 V. This increase of antiparallel conductance can be associated to an increase of the minority spin current which dominates in AP configuration. Its asymmetric shape is a signature of the different quality of the two barrier interfaces; this feature is then attributed to the contribution of the interfacial resonance state (IRS) lying in the minority band just above the Fermi level[1] at about 0.2 eV.[23,27] The existence of this interfacial state at the bottom interface of the barrier in sample A is attributed to its specific flatness quality (as shown in Figure 2) induced by high temperature annealing.

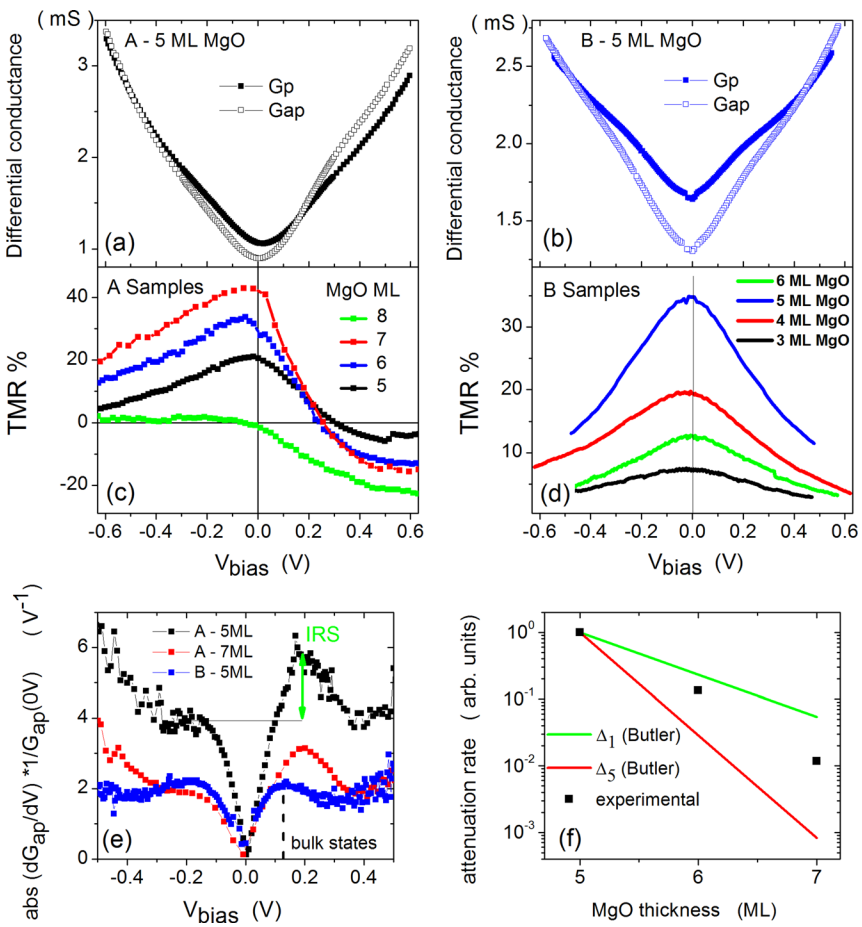

FIG. 4. Bias voltage dependence of: (a) and (b): parallel and antiparallel differential conductance, G_P and G_{AP}, for A-5 ML MgO and B-5 ML MgO samples, respectively; (c) and (d): TMR ratio for A and B-samples; (e): absolute value of the derivative of the differential antiparallel conductance. Figure 4(f): MgO thickness dependence of the attenuation rate of the IRS contribution in dG_{AP}/dV and from Ref. 1 referred to the 5 ML thickness.

This article is copyrighted as indicated in the article. Reuse of AIP content is subject to the terms at: http://scitation.aip.org/termsconditions. Downloaded to IP: 193.226.5.148 On: Wed, 14 May 2014 07:35:56

The TMR ratio is deduced from the resistance ($R = \frac{V}{I}$) measured in R_P and R_{AP} configuration: $TMR = \frac{R_{AP}-R_P}{R_P}$. The TMR(V) curve corresponding to A samples exhibits an asymmetrical shape with respect to B samples, with a striking sign reversal. These features can be readily interpreted in the light of the differential conductance behavior. This sign reversal is due to the activation of the minority IRS states as dominant transport channel in the AP configuration. As previously explained,[25] in that case, the competition between the positive spin polarization of bulk Fe with the negative polarization of the Fe/MgO interface provided by the minority IRS has to be considered. When the IRS is not contributing to tunneling transport (e.g., IRS quenched by roughness or not available at given energy), the positive spin polarization of the bulk Fe is usually dominating and results in a positive TMR. This can be observed in Figure 4(d) for B-samples in which the TMR has positive values for any V_{bias}. We note that in B-samples the absence of IRS states is furthermore confirmed from the differential conductivity measurements shown in Figure 4(b). In the asymptotic regime (thicker barrier), TMR reversal at low voltage has not been observed in standard Fe/MgO/Fe junctions[8,26,34] but has already been observed in interfacial carbon doped junction Fe-C/MgO/Fe.[30,35] In this last case, in agreement with theoretical calculations, the carbon doping enhances the minority IRS density at low voltage and its Δ_1 character. Thus, this enables the observation of minority IRS signature in tunnel transport although the MgO thickness is large and the Δ_1 symmetry is dominating the tunnel conductance. The signature of this IRS state exclusively in thinnest standard Fe/MgO/Fe junction suggests that it allows the propagation of symmetry states largely attenuated by the barrier, such as Δ_5, whose contribution is avoided in the asymptotic regime. Moreover, bulk states also contribute to the tunnel conduction.[8,26,30] To quantify the influence of IRS conduction, the derivative of G_{AP} has been plotted versus V_{bias} in Figure 4(e) for A and B samples. Assuming the absence of IRS signature on tunnel characteristics in B junctions, and in A junctions for negative voltage (when electrons are injected towards the top MgO/Fe interface, where the IRS is quenched by larger roughness), the contribution of the IRS can then be quantified by the asymmetric weight of the peak at +0.2 V, as shown by the green arrow in the figure. The weight of the IRS in $|\frac{dG_{AP}}{dV}|$ is presented in Figure 4(f) as a function of MgO thickness, with reference to the A-5 ML sample. It is compared to the theoretical attenuation rate of Δ_1 and Δ_5 symmetries.[1] The experimental points are observed to stay between the calculated attenuation rates for Δ_1 and Δ_5 symmetries, which indicate the symmetry mixing of this low energy IRS as theoretically predicted.[1,29] The presence of the Δ_1 component of this low voltage IRS, which is the only component evolved in the large barrier thicknesses regime, agrees with the observation of an asymmetric voltage dependence of the TMR in these junctions.[8,10] This Δ_1 minority conduction channel induced by the interface and located close to the Fermi level may contribute to the limited TMR ratio of the epitaxial junctions with respect to textured junctions.

The TMR dependence with MgO thickness is also revealed in Figures 4(c) and 4(d). The TMR increases (spin filtering increases) with MgO barrier thickness (from 5 ML to 7 ML and 3 ML to 5 ML in A- and B-samples, respectively) as expected.[1] We come back now to the anomaly found in Figure 3, where we analyzed the resistance area-product (R_pA) variation with MgO thickness (t_{MgO}). The sudden decrease of log (R_pA) from the expected linear variation with t_{MgO}, observed for the thickest barrier of both A and B junctions, corresponds in Figure 4 to the sudden decrease of the TMR versus t_{MgO}. Such non-monotonic dependence of R_pA and TMR with MgO thickness has already been reported in Fe/MgO single crystal MTJs.[36] We propose to associate these features with a decrease of the MgO barrier quality for a peculiar thickness. This could be related to the specific properties of MgO epitaxial growth on (001) Fe, induced by their relative lattice mismatch. During the deposition of the first layers, the growth is pseudomorphic: MgO adopts the in-plane lattice parameter of Fe. Due to the strain energy, above a critical thickness, the plastic relaxation occurs: MgO recovers its own lattice parameter with the introduction of extended defects as dislocations.[19,34] The detrimental contribution of these defects to transport properties in Fe/MgO/Fe junctions has been clearly reported.[19,34] Moreover, this relaxation depends obviously on growth conditions: it occurs at a larger deposited thickness for a lower deposition temperature, when the layer by layer growth is more effective (with less damped RHEED intensity oscillations).[3] In the present study, the MgO growth conditions are governed by the quality of the initial Fe surface which are obviously optimized for A-samples with respect to B, as illustrated in Figures 2(a)–2(d). As a result, MgO layer by layer growth is better controlled in A-samples, as illustrated with RHEED intensity oscillations in Figure 2(e). This would be coherent with a larger expected critical thickness for the MgO plastic relaxation in A-samples (≈8 ML), than in B-samples (≈6 ML). Furthermore, above these critical thicknesses, the dislocations will always exist in the MgO barrier and will play a negative role on spin and symmetry filtering efficiency. However, due to limited density of dislocations and existence of perfect structural coherent zones within Fe/MgO/Fe MTJs,[20] the global symmetry filtering efficiency of the MgO barrier increases with barrier thickness. This explain the subsequent experimentally observed enhancement of TMR with barrier thickness in the asymptotic regime,[8] as theoretically predicted by Butler *et al.*[1,2]

In summary, the transport properties of epitaxial Fe/MgO/Fe junctions have been investigated in the low thickness barrier regime (3 ML to 8 ML), where poor symmetry filtering by the MgO barrier enable analysis of tunnel transport channels quenched at large MgO thickness (asymptotic regime). Therefore, we were able to analyze specific signature of Δ_5 conduction channel. A tunnel magnetoresistance sign reversal at low voltage due to the contribution of the Fe/MgO interfacial resonant state located in the minority band close above the Fermi level has been observed. Moreover, the analysis of MgO thickness dependence of the antiparallel conductivity indicates a mixing symmetry character Δ_1-type + Δ_5-type of this IRS. The Δ_1-type component of this low voltage IRS may contribute to the limitation of the TMR in junctions with a larger MgO thickness. As a consequence, the possibility of tuning this IRS towards higher

This article is copyrighted as indicated in the article. Reuse of AIP content is subject to the terms at: http://scitation.aip.org/termsconditions. Downloaded to IP: 193.226.5.148 On: Wed, 14 May 2014 07:35:56

energy level or towards Δ_5 symmetry by chemical or structural interface engineering would be interesting to explore.

Dr. Ramesh Babu Gangineni would like to thank Delaye Marie-Thérèse for her help in training the nano-fabrication techniques. C. Tiusan acknowledges the following projects: SPINCHAT (ANR-07-BLAN-341), POS CCE ID. 574, code SMIS-CSNR 12467, and the Exploratory Research Project "SPINTAIL" PN-II-ID-PCE-2012-4-0315, No. 23/29.08.2013.

[1]W. H. Butler, X.-G. Zhang, T. C. Schulthess, and J. M. MacLaren, Phys. Rev. B **63**(5), 054416 (2001).
[2]J. Mathon and A. Umerski, Phys. Rev. B **63**, 220403(R) (2001).
[3]J. L. Vassent, M. Dynna, A. Marty, B. Gilles, and G. Patrat, J. Appl. Phys. **80**(10), 5727 (1996).
[4]M. Klaua, D. Ullmann, J. Barthel, W. Wulfhekel, J. Kirschner, R. Urban, T. L. Monchesky, A. Enders, J. F. Cochran, and B. Heinrich, Phys. Rev. B **64**, 134411 (2001).
[5]S. Yuasa, T. Nagahama, A. Fukushima, Y. Suzuki, and K. Ando, Nat. Mater. **3**, 868 (2004).
[6]S. S. P. Parkin, C. Kaiser, A. Panchula, P. M. Rice, B. Hughes, M. Samant, and S.-H. Yang, Nat. Mater. **3**, 862 (2004).
[7]S. Yuasa, A. Fukushima, H. Kubota, Y. Suzuki, and K. Ando, Appl. Phys. Lett. **89**, 042505 (2006).
[8]C. Tiusan, M. Hehn, F. Montaigne, F. Greullet, S. Andrieu, and A. Schuhl, J. Phys.: Condens. Matter **19**, 165201 (2007).
[9]S. Ikeda, J. Hayakawa, Y. Ashizawa, Y. Lee, K. Miura, H. Hasegawa, M. Tsunoda, F. Matsukura, and H. Ohno, Appl. Phys. Lett. **93**, 082508 (2008).
[10]A. Duluard, B. Negulescu, C. Bellouard, M. Hehn, D. Lacour, Y. Lu, G. Lengaigne, F. Montaigne, S. Robert, S. Suire, and C. Tiusan, Appl. Phys. Lett. **100**, 072408 (2012).
[11]P. G. Mather, J. C. Read, and R. A. Buhrman, Phys. Rev. B **73**, 205412 (2006).
[12]G. X. Miao, Y. J. Park, J. S. Moodera, M. Seibt, G. Eilers, and M. Münzenberg, Phys. Rev. Lett. **100**, 246803 (2008).
[13]J. P. Velev, K. D. Belashchenko, S. S. Jaswal, and E. Y. Tsymbal, Appl. Phys. Lett. **90**, 072502 (2007).
[14]C. Wang, A. Kohn, S. G. Wang, L. Chang, S.-Y. Choi, A. Kirkland, A. K. Petford-Long, and R. C. C. Ward, Phys. Rev. B **82**, 024428 (2010).
[15]H. Meyerheim, R. Popescu, J. Kirschner, N. Jedrecy, M. Sauvage-Simkin, B. Heinrich, and R. Pinchaux, Phys. Rev. Lett. **87**, 076102 (2001).
[16]X.-G. Zhang, W. H. Butler, and A. Bandyopadhyay, Phys. Rev. B **68**, 092402 (2003).
[17]S. G. Wang, G. Han, G. H. Yu, Y. Jiang, C. Wang, A. Kohn, and R. C. C. Ward, J. Magn. Magn. Mater. **310**, 1935 (2007).
[18]P. Luches, S. Benedetti, M. Liberati, F. Boscherini, I. I. Pronin, and S. Valeri, Surf. Sci. **583**, 191 (2005).
[19]F. Bonell, S. Andrieu, C. Tiusan, F. Montaigne, E. Snoeck, B. Belhadji, L. Calmels, F. Bertran, P. Le Fevre, and A. Taleb-Ibrahimi, Phys. Rev. B **82**(9), 092405 (2010).
[20]M. S. Gabor, C. Tiusan, T. Petrisor, Jr., T. Petrisor, M. Hehn, Y. Lu, and E. Snoeck, J. Magn. Magn. Mater. **347**, 79–85 (2013).
[21]A. Biedermann, O. Genser, W. Hebenstreit, M. Schmid, J. Redinger, R. Podloucky, and P. Varga, Phys. Rev. Lett. **76**, 4179 (1996).
[22]N. Papanikolaou, B. Nonas, S. Heinze, R. Zeller, and P. H. Dederichs, Phys. Rev. B **62**, 11118 (2000).
[23]J. A. Stroscio, D. T. Pierce, A. Davies, R. Celotta, and M. Weinert, Phys. Rev. Lett. **75**, 2960 (1995).
[24]P. H. Dederichs, P. Mavropoulos, O. Wunnicke, N. Papanikolaou, V. Bellini, R. Zeller, V. Drchal, and J. Kudrnovský, J. Magn. Magn. Mater. **240**, 108 (2002).
[25]C. Tiusan, J. Faure-Vincent, C. Bellouard, M. Hehn, E. Jouguelet, and A. Schuhl, Phys. Rev. Lett. **93**, 106602 (2004).
[26]P.-J. Zermatten, G. Gaudin, G. Maris, M. Miron, A. Schuhl, C. Tiusan, F. Greullet, and M. Hehn, Phys. Rev. B **78**, 033301 (2008).
[27]M. M. J. Bischoff, C. Konvicka, A. J. Quinn, M. Schmid, J. Redinger, R. Podloucky, P. Varga, and H. van Kempen, Phys. Rev. B **68**, 045422 (2003).
[28]T. X. Wang, Y. Li, K. J. Lee, J. U. Cho, D. K. Kim, S. J. Noh, and Y. K. Kim, J. Appl. Phys. **109**, 083714 (2011).
[29]C. Uiberacker and P. M. Levy, Phys. Rev. B **64**, 193404 (2001).
[30]Y. Lu, H.-X. Yang, C. Tiusan, M. Hehn, M. Chshiev, A. Duluard, B. Kierren, G. Lengaigne, D. Lacour, C. Bellouard, and F. Montaigne, Phys. Rev. B **86**, 184420 (2012).
[31]J. C. Sankey, Y.-T. Cu, J. Z. Sun, J. C. Slonczewski, R. A. Buhrman, and D. C. Ralph, Nat. Phys. **4**, 67 (2008).
[32]H. Kubota, A. Fukushima, K. Yakushiji, T. Nagahama, S. Yuasa, K. Ando, H. Maehara, Y. Nagamine, K. Tsunekawa, D. D. Djayaprawira, N. Watanabe, and Y. Suzuki, Nat. Phys. **4**, 37 (2008).
[33]J. Z. Sun and D. C. Ralph, J. Magn. Magn. Mater. **320**, 1227 (2008).
[34]F. Bonell, S. Andrieu, F. Bertran, P. Lefevre, A. T. Ibrahimi, E. Snoeck, C. Tiusan, and F. Montaigne, IEEE Trans. Magn. **45**(10), 3467 (2009).
[35]C. Tiusan, M. Sicot, M. Hehn, C. Belouard, S. Andrieu, F. Montaigne, and A. Schuhl, Appl. Phys. Lett. **88**, 62512 (2006).
[36]R. Matsumoto, A. Fukushima, K. Yakushiji, S. Yakata, T. Nagahama, H. Kubota, T. Katayama, Y. Suzuki, K. Ando, S. Yuasa, B. Georges, V. Cros, J. Grollier, and A. Fert, Phys. Rev. B **80**, 174405 (2009).

This article is copyrighted as indicated in the article. Reuse of AIP content is subject to the terms at: http://scitation.aip.org/termsconditions. Downloaded to IP: 193.226.5.148 On: Wed, 14 May 2014 07:35:56